

Dislocation–Assisted Initiation of Energetic Materials*

Ronald W. Armstrong
Center for Energetic Concepts Development
University of Maryland, College Park, MD 20742, U.S.A.

Abstract

The role of dislocations in assisting initiation of (explosive) chemical decomposition of energetic materials has connection with the known influences for crystals and polycrystals of dislocations facilitating permanent deformations and phase transformations. X-ray topographic observation of relatively few dislocations in solution-grown crystals relates to the influence of large Burgers (displacement) vectors that are characteristic of molecular crystal bonding. Both model evaluations of the load dependence of cracking at hardness indentations and the derived hardness stress-strain behaviors show that dislocation movement is difficult whether in the indentation strain fields or at the tips of indentation-induced cracks. Thus, energetic crystals are elastically compliant, plastically hard, and relatively brittle [1]. Nevertheless, cracking is shown to be facilitated by the shear stress driven, normally limited, dislocation flow that, on molecular dynamics and dislocation pile-up model bases, is shown to be especially prone to producing localized hot spot heating for explosive initiations. Such model consideration is in agreement with greater drop-weight heights being required to initiate smaller crystals. The crystal size effect carries over to more difficult combustion occurring for compaction of smaller crystals. The total results relate to dual advantages of greater strength and reduced mechanical sensitivity accruing for the development of nanocrystal formulations. In consequence, also, several levels of dislocation-assisted modeling are described for initiation mechanisms under shock wave loading conditions.

1. Dislocation origins in energetic crystals

The crystallographically imperfect structures of conventional, solution grown, energetic crystals, for example, of RDX (cyclotrimethylenetrinitramine), show a segmented growth sector structure in agreement with dislocation-based crystal growth predictions [2], as shown in Figure 1a-d. In 1a, first, a cross-sectional sketch is shown of the overall growth sector and boundary structure that is normally developed during progressive growth of a polygonally-shaped crystal and, in 1b, is shown separately the threading dislocation “bundle” structure emanating from a crystal seed, S. The dislocations produce crystal growth more easily than any other mechanism. As indicated in 1b, the dislocation bundles may emanate from inclusion particles. Profuse nucleation of such dislocation bundles was shown to occur at interrupted sapphire crystal growth surfaces via x-ray diffraction topographic imaging of crystal sections [3]. Here, a tabular RDX crystal sectioned parallel to its planar (001) top/bottom surface [4] is shown in Figure 1c.

***Proceedings of 8th International Seminar: *New Trends in Research of Energetic Materials*, J. Vagenknecht, ed., Univ. Pardubice, CZ, 2005, Part 1, pp. 28-43; *Central European Journal of Energetic Materials (CEJEM)*, **2**, [2], in print.**

The crystallographic labels in the Figure were identified from angular measurements on a standard (001) stereographic projection for the RDX orthorhombic lattice [5]. The growth sector boundaries provide sinks for solute pushed laterally during the facet-sensitive extension of the adjacent growth sector regions along their normal, \mathbf{n}_i , directions in accordance with locally-operative temperature and solute gradients that can be different at adjacent \mathbf{n}_i levels.

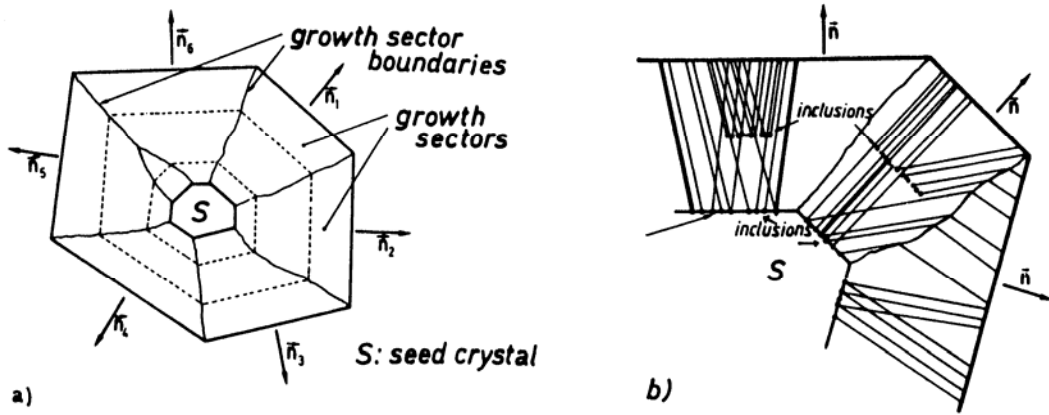


Figure 1a. From Klapper [2], showing growth sectors and boundaries building onto a seed; and, 1b. Growth-promoting dislocation lines emanating from seed and inclusions.

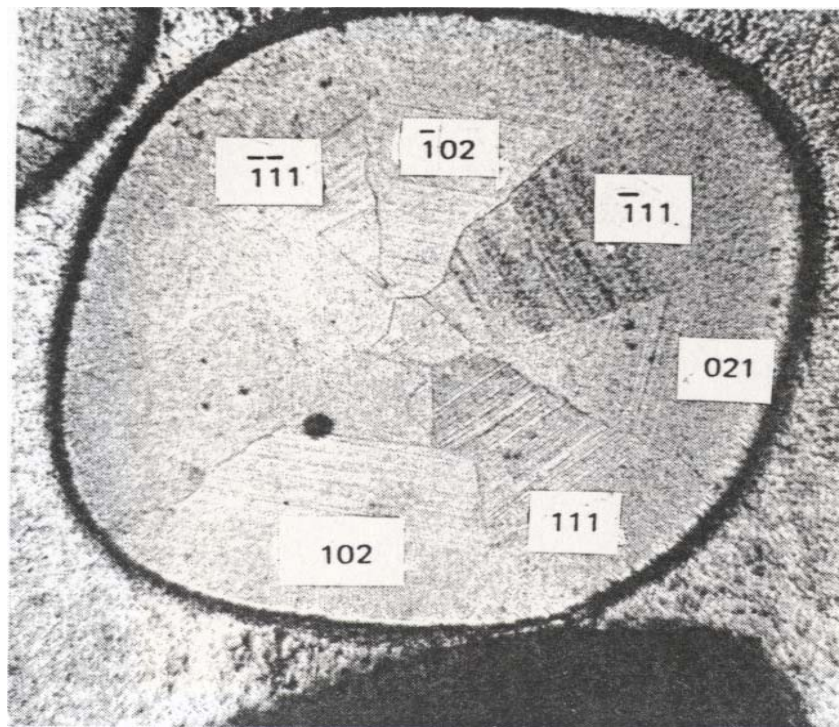


Figure 1c. An (001) sectioned RDX crystal [4], after chemical polishing, with identified traces [5] of the original polygonal crystal growth surfaces at earlier stages of growth.

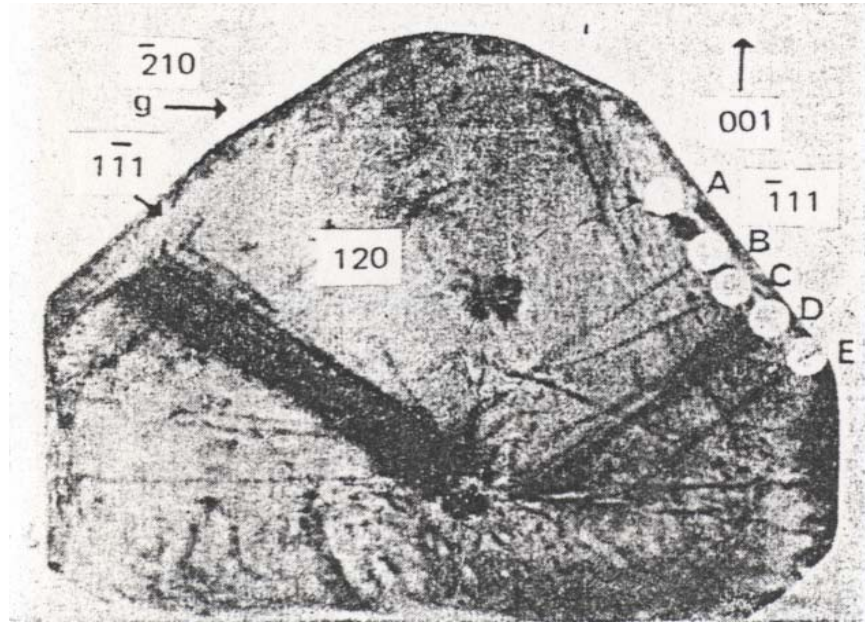


Figure 1d. A $\{210\}$ type Lang transmission x-ray diffraction topograph of an RDX crystal slice showing dislocation bundles emanating from a central crystal seed [6].

The black lines in Figure 1d, relating to the schematic dislocation lines in Figure 1b, are revealed because of the dislocation strain fields locally enhancing in their vicinity the diffracted x-ray intensity [7], much the same as “thinner” dislocation lines are observed in metals through transmission electron microscopy. In Figure 1d, small metal spheres, shown as white circles, had been put into etch pit depressions on the right-hand $\{111\}$ type crystal facet to confirm that any dislocation lines revealed in the topographic images would run into the pits, as shown.

Thus, energetic crystals, as all others, contain an intrinsic population of dislocations that play an intimate role in the crystal formation process. The special nature of the dislocations in molecularly bonded energetic crystals, however, relates first to the dislocation self-energy, E_s expressed as:

$$E_s = [G b^2 / 4\pi\alpha] \ln [R/r_0] + E_c \quad (1)$$

where G is the shear modulus; b is the dislocation Burgers (displacement) vector; α is a factor depending on whether the dislocation is of screw ($\alpha = 1$), edge ($\alpha = [1-\nu]$), or mixed type; ν is Poissons ratio; R is an outer cut-off radius for negligible displacement compared to lattice vibrations; r_0 is an inner core cut-off radius determined by the limit of linear elasticity; and E_c is the remaining dislocation core energy [8]. For the molecularly-bonded energetic crystals compared to others, the large value of b outweighs the lower value of G , and so the dislocation self-energies are relatively large [9]. The

consequence is that energetic crystals generally contain few dislocations --- but as will be seen, the dislocation influence on strength properties and plastically-generated hot spots is large [1].

2. Indentation properties

The known brittleness of energetic crystals promoted early measurements being made of their cracking behaviors by the method of indentation fracture mechanics (IFM) [10]. Figure 2 is a comparison on a log-log basis of measured diamond pyramid indentation diagonal lengths and tip-to-tip crack lengths (along the diagonals) produced at different load values [11 -14].

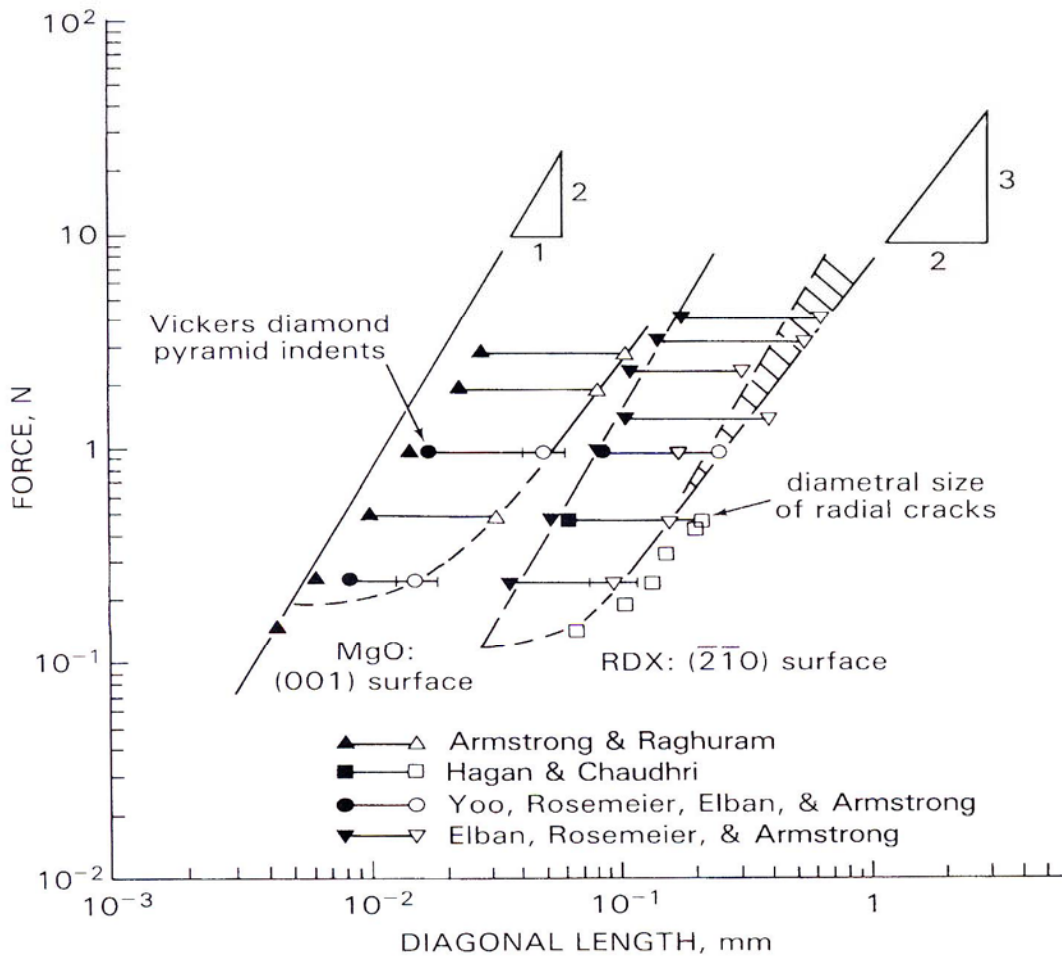


Figure 2. A comparison between MgO and RDX of loading force versus indentation diagonal and tip-to-tip (diagonal) crack lengths for assessment of cracking behaviors.

In Figure 2, obtainment of a constant Vickers diamond pyramid hardness would be indicated by a line of slope 2.0 as indicated by the line with that slope drawn to the left-side triangle. For the MgO result, cracking occurred at the second highest applied load

of 25 g. and produced the indicated trend of a reduced hardness continuing to occur at increasing load values. In Figure 2, RDX is shown to have a lower hardness than MgO because of the downward shifted parallel line of slope 2.0 for RDX and also is shown to be more brittle than MgO because of cracking occurring at the lowest applied load of 15g. The important characterization of cracking for the two materials in Figure 2, however, relates to the prediction of a slope of 1.5 for the load dependence on crack size predicted on an IFM basis [10, 15]. For the MgO measurements, a reasonable fit to the IFM prediction is seen to apply at the larger applied loads and, moreover, the occurrence of cracking has apparently influenced the plastic hardness value in the same manner. Alternatively, the RDX crack size measurements appear to show a slope value greater than 1.5, perhaps approaching 2.0, as indicated for the hardness measurements themselves. Furthermore, an IFM analysis by Elban [16] of the Hagan and Chaudhri [12] cracking measurements gave the important result that relatively little plastic flow was produced at the crack tips.

Further assessment of the relative hardness and cracking properties of RDX is able to be made on the basis of the relation between the hardness pressures and the effective hardness strains associated with those pressures. Figure 3 shows such a comparison.

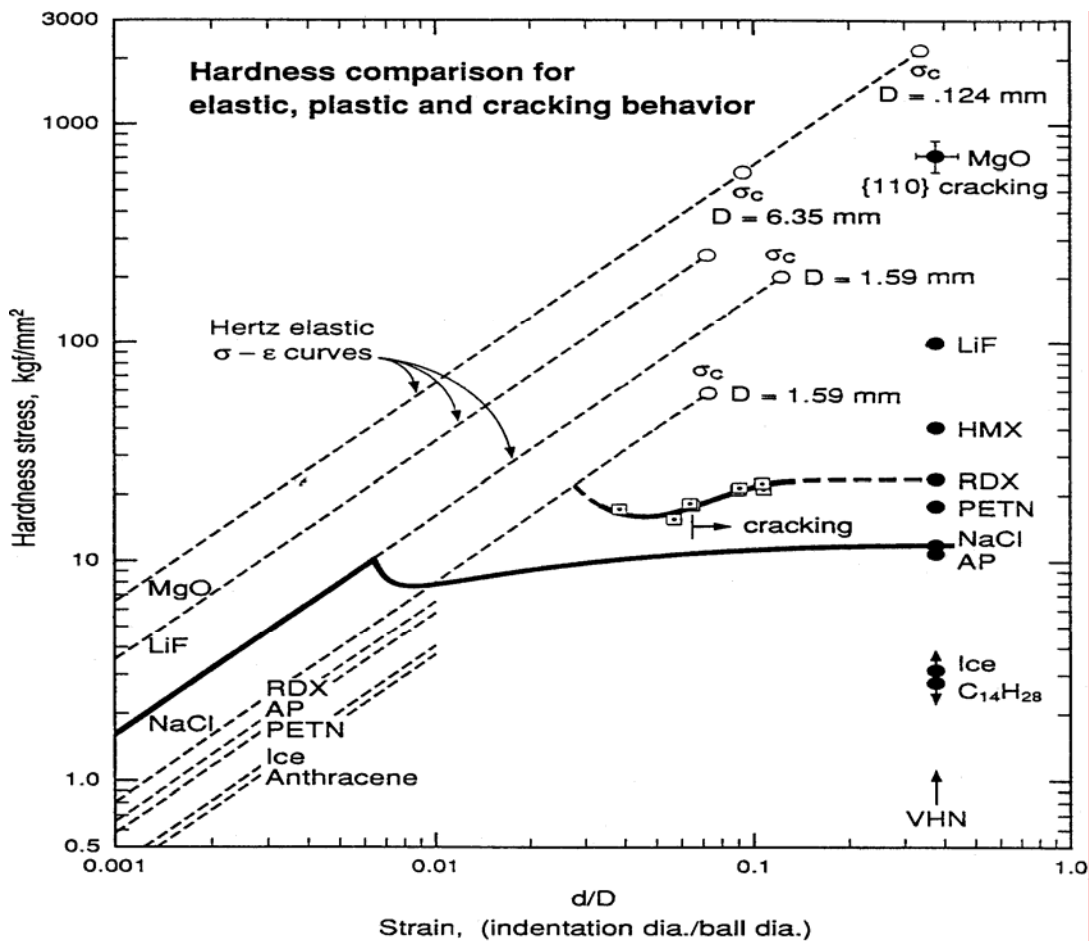


Figure 3. Elastic/plastic/hardness stress-strain comparison among different materials

In Figure 3, that is based on a hardness stress-strain description given by Hammond and Armstrong [17], the hardness stress is defined on the basis of a ball indentation test as the applied load divided by the projected circular area of contact with the material surface. The hardness strain is specified as the contact diameter, d , divided by the ball diameter, D . Actual Vickers hardness numbers (VHN) are plotted in the Figure along a vertical range of values at an effective d/D value of 0.375. A number of conventional Meyer hardness measurements for RDX, made with a 1.59 mm ball diameter, are plotted as open-square points in the Figure [18]. A linear dependence of hardness stress, σ on (d/D) is predicted for elastic loading according to the Hertzian relationship

$$\sigma_H = (4/3\pi) [\{(1-\nu_m^2)/E_m\} + \{(1-\nu_b^2)/E_b\}]^{-1} (d/D) \quad (2)$$

where ν_m , E_m and ν_b , E_b are the Poissons ratios and Young's modulus values for the tested material and ball, respectively. The straight dashed lines shown at the left-side of the Figure were computed for the listed materials while the heavy line result for NaCl, even extending laterally to a comparable (d/D) value to the VHN measurement, was determined from points taken along a continuous indentation test [19]. At the upper terminal points of the lines are given σ_C values that represent the IFM cracking stresses to be achieved on elastic loading in accordance with the relationship [20]

$$\sigma_C = [4E_m\gamma/\{\pi D(1 - \nu_s^2)(K_1^2 + K_2^2)\}]^{1/2} (d/D)^{-1/2} \quad (3)$$

where γ is the crack surface energy and $(K_1^2 + K_2^2)$ is a numerical factor equal to 2.5×10^{-5} . As indicated in equation (3) and along the loading line for MgO in Figure 2, a lower value of σ_C is obtained at larger D values. The topmost 0.124 mm D value indicated on the MgO line is an equivalent ball diameter corresponding to the VHN indentation size.

Among the various material identifying labels in Figure 3 are those, in addition to RDX, for PETN (pentaerythritol tetranitrate), AP (ammonium perchlorate), and HMX (cyclotetramethylenetetranitramine). Whereas ionic-bonded AP has approximately the same VHN hardness as NaCl, the hardnesses of PETN, RDX and HMX are increasingly greater in that order. The result is interesting to compare with the material elastic stiffnesses that are included in the bracketed effective modulus factor in equation (2). Thus, as expected the Young's modulus, E_m , for PETN and RDX are indicated to be significantly lower in Figure 3 than E_m for NaCl, compared to the reversed result for the VHN measurements and the ball test points for RDX. The comparison between elastic moduli and measured hardnesses provides a basis for the assertion that energetic crystals are relatively hard. Also, in all cases, the measured hardnesses are lower than the theoretical stresses required for cracking in the absence of plastic flow. The experimental hardness points for RDX show that cracking occurs after significant plastic flow has occurred. Thus, whereas the presence of dislocations allows plastic flow to occur at lower stresses than would result in their absence, the dislocation motion also provides cracking at lower stresses than would result only from elastic deformation!

Modeled dislocation displacements in RDX have shown, in general, that shearing displacements and, hence, dislocation movement are difficult because of the intertwined nature of the oddly shaped molecules otherwise packed into relatively dense crystal structures [21, 22]. Figure 4 shows an example for the projection of slip (in and out of the Figure) in the [100] direction on the {021} type slip plane in the orthorhombic RDX lattice

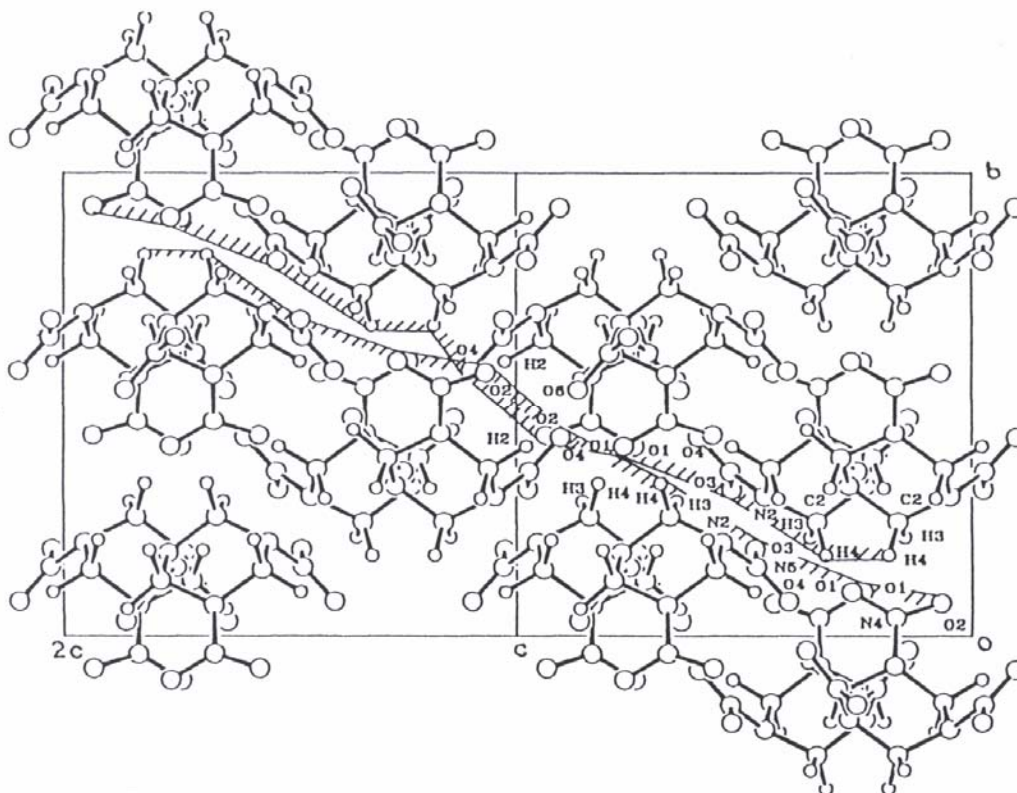


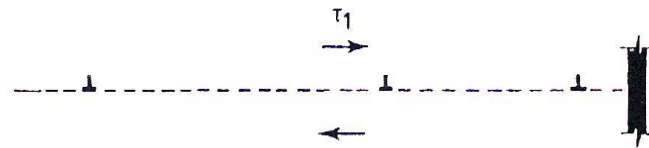
Figure 4. An a-axis [100] projection, of the eight RDX molecule positions in each of two adjacent unit cells, shown in the (100) plane containing the horizontal c-axis [001] direction (to the left) and the b-axis [010] direction vertical, also with labeled hydrogen, oxygen and nitrogen atom position obstructions near to the crystal {021} type slip plane.

An important aspect of such modeling of shear displacements, as shown in Figure 4, is to show that, beyond mutual blockages between adjacent molecules, their forced shearing in dislocation motion can bring the respective outcropping intermolecular appendages into critical reaction coordinate separations. For the case projected in Figure 4 near to the cell coordinate position (0,0.5,1), the hydrogen-oxygen interactions could promote nitroso compound formations as have been detected both in partially initiated material recovered from drop-weight impact tests [23] and in combustion residues [24]. Such forced shearing of molecules to achieve chemical decomposition obviates the more difficult requirement of imposing greater hydrostatic pressures to achieve the same

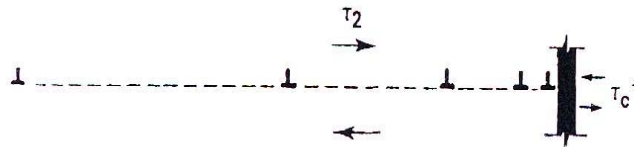
atomic separations. Gilman [25] has emphasized the importance of elastic shear strains even, compared to hydrostatic ones, in facilitating chemical reactions.

3. Drop-weight impact sensitivity

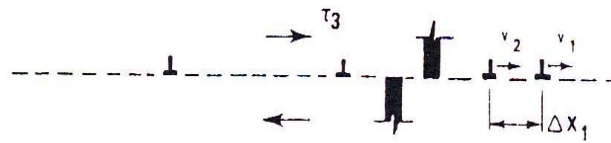
Early work on drop-weight impact testing of energetic crystal powders led to the model of converting the plastic work to hot spot heating for material initiation [26]. In further research measuring the strain responses in drop weight impact tests performed on a wide variety of materials, Heavens and Field [27] found that explosive decompositions were associated with discontinuous drops in load occurring during the material loading. Such load-drop behavior is well-known in the materials community and is associated with dislocation pile-up behavior [28], as shown schematically in Figure 5, although attention



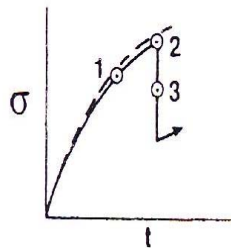
(a) isothermal stress build-up: n_1 dislocations



(b) critical stress concentration: $n_2 \tau_2 = \tau_c^*$



(c) adiabatic collapse-discontinuous load drop



(d) pressure-time curve for τ_1 , τ_2 , and τ_3

Figure 5. Dislocation pile-up avalanche model for quick dissipation of stored energy [28].

had not been previously directed to the thermal energy release attending pile-up breakthroughs. After essentially isothermal build-up of internal energy in the pile-up, as indicated in Figure 5a, a critical condition for pile-up release is achieved, as depicted in Figure 5b whereupon the dislocations are driven past the collapsed obstacle by an internal stress magnified by the number of dislocations in the pile-up. The critical breakthrough condition of Figure 5b involves the number of dislocations, n_2 , that is linearly proportional to the slip length, ℓ , and τ_2 , so that for τ_c^* being determined by a constant localized stress requirement, say, for cracking, then

$$\tau_2 = \tau_0 + [c \sqrt{(G \tau_c^* b)}] \ell^{-1/2} \quad (4)$$

where τ_0 is the shear stress required for intrinsic dislocation movement, c is a numerical constant, and the other symbols have been defined in equation (1). Such reciprocal

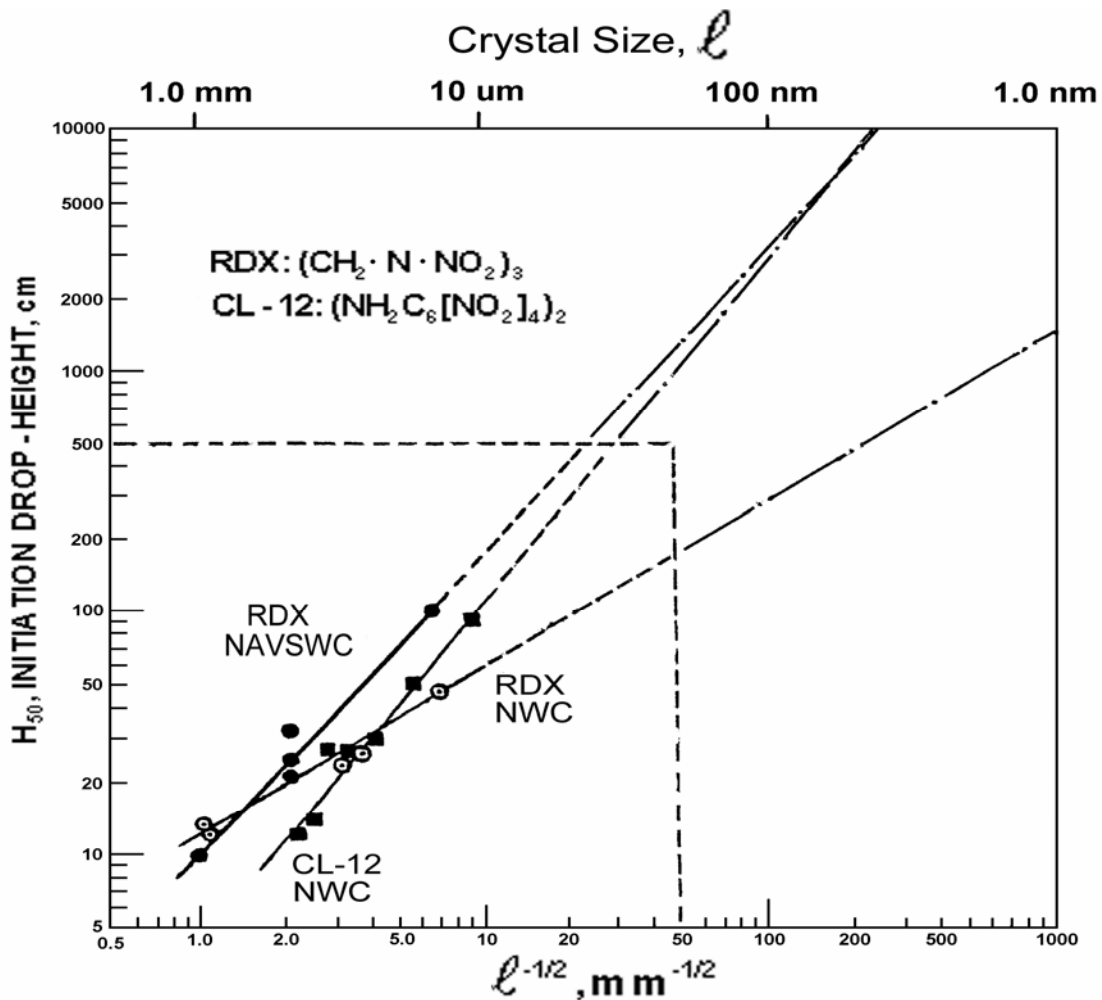


Figure 6. Initiation drop-weight height versus $\ell^{-1/2}$, extended to nano-scale crystal sizes.

square root of slip length dependence for the applied shear stress is known as a Hall-Petch (H-P) dependence after these researchers independently measured such dependencies for the plastic yield stress and cleavage fracture stresses of steel materials that, not incidentally, normally exhibit sudden load drop behavior during their initial yielding behaviors. The rather broad application of such pile-up theory for explaining the influence of grain size on the mechanical properties of materials has been recently reviewed [29]. The model consideration of Figure 5, involving the grain size dependence described in equation (4), was employed with addition of a thermally-activated model for the intrinsic dislocation movement, to give a log-log dependence for the drop-weight sensitivity for 50% probability of initiation, H_{50} , and $\ell^{-1/2}$, with ℓ taken as the crystal particle size [1, 30]. Figure 6 presents those results and added ones [31] for other RDX and CL-12 crystals. The dashed lines in the Figure enclose a region of crystal sizes larger than $0.4 \mu\text{m}$, and the extension of the Figure has been made to indicate, by extrapolation, the regime of mechanical insensitivity that might be achievable with nanometric-sized crystals. Some supporting evidence for improved crystal insensitivities at nanocrystal sizes has been presented [32]. Also, such indication in Figures 5 and 6 of importance of the dislocation loading rate, it being greater for greater drop-weight heights, relates to Figure 3 where the plastic and cracking hardness stress results for RDX show that there is not a very large range in stress levels available for investigation of the dynamic strain rate dependence of dislocation behavior. And, furthermore, the number of dislocations required in a pile-up to produce cracking in RDX is not very great either, hence, relating to the intrinsic brittleness of RDX, as assessed earlier by Armstrong and Elban [9] in terms of the dislocation self-energy and the surface energy for cracking, including its experimental determination on an IFM basis [16].

4. Combustion

The cracking behavior of RDX and related energetic crystals is of interest for thermal stress influences during combustion of conventional energetic material formulations that, generally, incorporate polymer binding materials and a small amount of surfactants. The crystals themselves burn over a melt layer formed on their surfaces. Figure 7 shows evidence of such result at a burn spot produced with a laser beam shone onto the surface of an isolated RDX crystal [33]. The relatively low energy beam was directed onto the crystal surface at a low glancing angle. The outer elliptical extent of the melt spot is made recognizable by a network of fine cracks separated vertically by $\sim 5 \mu\text{m}$. Their occurrence was explained [18] in terms of the thermal stresses more easily producing cracking under the melt layer because then only the liquid-solid interfacial energy had to be supplied for cracking as compared with the vapor-solid γ value outside of the melt spot. Such consideration was employed on a conventional fracture mechanics basis, also, to inquire whether such cracking could be responsible for a pressure-induced instability of the energetic material burn rates through the crack magnification of induced burn rate pressures [34].

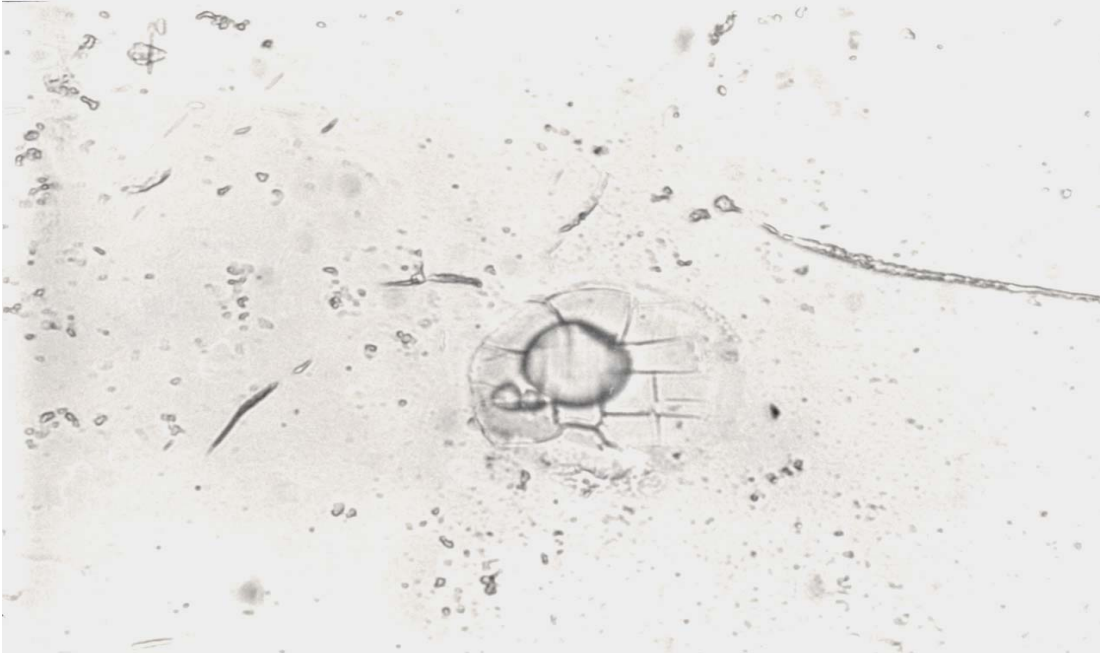


Figure 7. A laser-beam-induced melt spot produced on an RDX crystal surface with thermally induced cracking having occurred underneath the crystal melted layer [33].

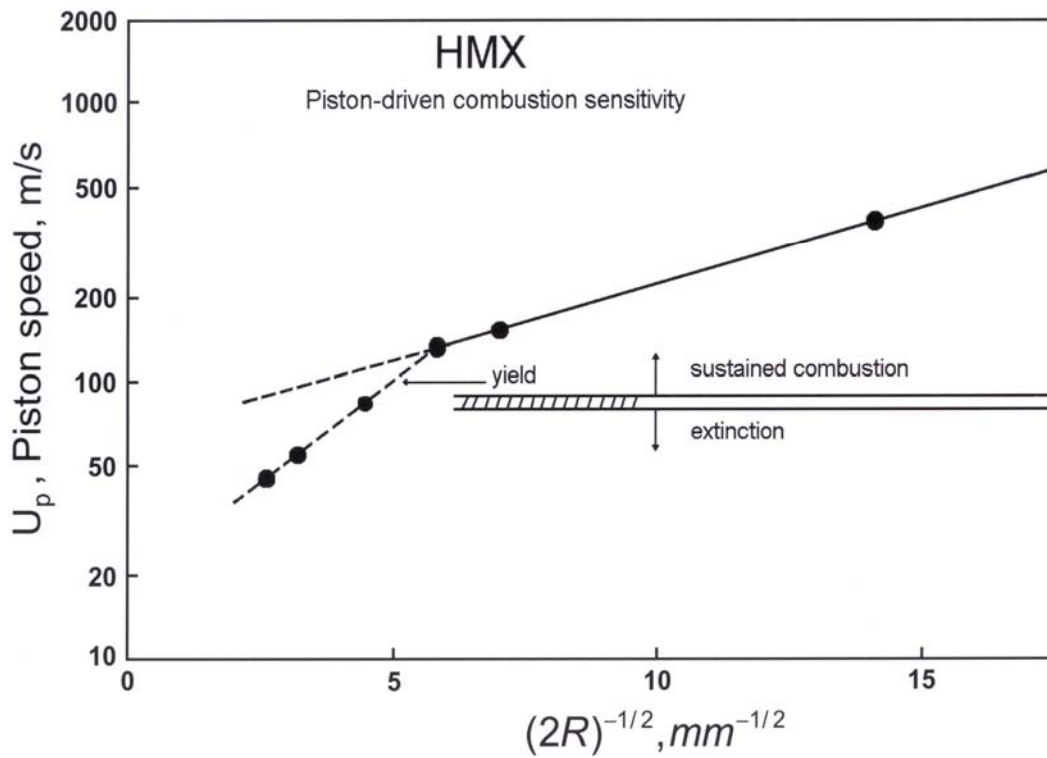


Figure 8. HMX particle size dependence of combustion initiated during modeled piston-driven compaction, after computed results presented by Gonthier [35].

Another aspect of particle size influence, this time, on the combustion behavior of energetic materials is indicated in the modified H-P type dependence; see equation (4) in Section 3; now shown in Figure 8 derived from computations presented by Gonthier for the piston-driven compaction of a granular bed [35]. The computational model was based on experimental results reported by Jacobs, Sandusky and Elban [36] for particle diameters of size, $2R$. The demarcation between extinction versus sustained combustion was associated with the boundary between local deformation and full particle-to-particle yielding of the compressed bed. In this case, the thermally activated model of dislocation motion mentioned with respect to the particle size dependence in Figure 6, where $l = 2R$, generally gives a logarithmic dependence on imposed strain rate of the thermal stress and, so, the expectation of a linear H-P type dependence in Figure 8, following equation (4) if transmission of plastic flow through the particle bed is required to sustain combustion.

5. Shock effects

The limit of imposed deformation rate on dislocation behavior in crystals and polycrystals is achieved with the propagation of a shock wave. A recent symposium has been concerned with understanding such influence, mostly, on structural metals and alloys [37]. Pioneering results had been reported by Smith [38]. The Hugoniot

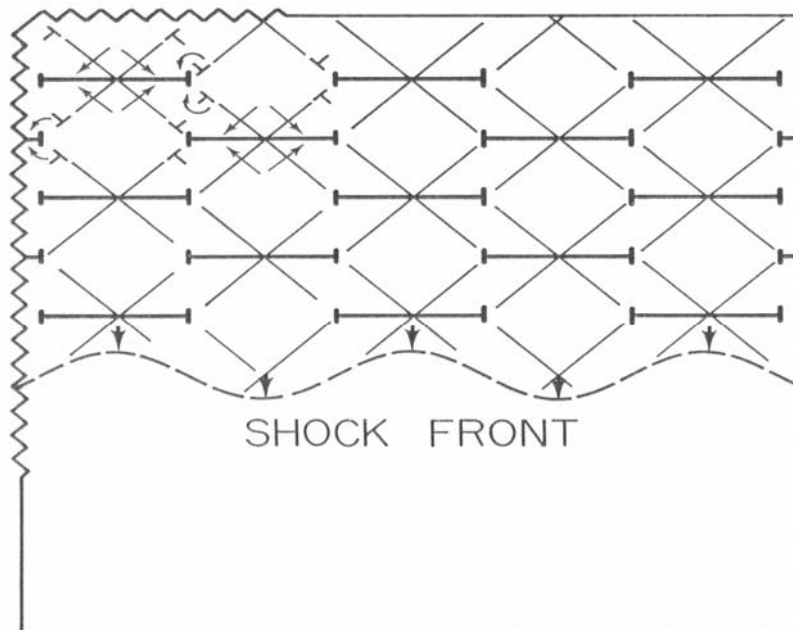


Figure 9. Model for nanometer-scale dislocation generation at a shock front [43-45].

elastic limit (HEL) stress for shock-induced yielding of Armco iron material has been shown to follow an H-P dependence [39, 40]. There is equal concern about understanding shock wave influences on the properties of energetic crystals, including their initiations [5, 41]. Concern has been expressed for the shock propagation front moving too fast for thermally activated chemical reactions to occur [42].

A broadly applicable model for achieving a residual state of one-dimensional strain at the shock front has been described [43], as shown in Figure 9, and elaborated [44, 45]. A fine scale dislocation structure is generated at the shock front for two reasons: (1) the significant shear strain magnitudes developed at the shock front are not able to be relieved by the displacement, at some distance away, of the intrinsic dislocation population; and, (2) the resident dislocation population can only travel, at fastest, at a slower elastic wave speed. The shock front itself is envisioned to have a width on the scale of nanometers. As indicated in Figure 9, dislocation loops form on conjugate shear planes and then intersect to react, presumably, after nanoscale movement to produce an immobile network of interstitial-type prismatic dislocation loops with Burgers vectors parallel to the direction of shock wave propagation. The dislocation network is available for interaction with the resident dislocation population traveling behind the shock front. The interaction has been proposed to provide analogous behavior to that established in neutron irradiation experiments, for example, leading to dislocation channeling because of follow-on further reactions between the shock-generated dislocation network and the original resident dislocations [1, 5]. Shock hardening in copper in post-shock deformation experiments is well-established and attributed to the presence of a shock-induced defect structure [46].

Because of the small material volume involved at the shock front, and short time for wave passage, the subject lends itself to description of individual atomic or molecular force interactions via the method of molecular dynamics (MD) [47]. Of particular concern has been the influence of such fast compression on defects such as voids. An important result obtained for collapse of a void in a simple atomic lattice into a dislocation defect structure [48] has been the observation that such permanent relaxation converted the higher potential energy of atoms adjacent to the void into thermal hot spot energy, thus, giving evidence that such permanent deformation process always generates significant thermal energy above the normal atomic lattice modes. Recent model computations have been presented for large-scale MD simulation of the orientation dependence of shock deformations in a face-centered-cubic lattice [49]. Such experiments possibly relate to pioneering measurements made on the orientation dependence of “run-to-detonation” measurements made on body-centered-tetragonal PETN crystals by Dick and attributed by him to the orientation dependence of shearing actions in the perfect lattice [50], akin to the model considerations given in references [21] and [22].

Acknowledgements

The present article has drawn heavily on reference [1] with benefit from association with my co-author there, Wayne Elban. Again, appreciation is expressed both to Byron Allmon for help given in compiling Figures; and to the following agencies who have supported the overall research effort: the Office of Naval Research, at Arlington, VA; the Naval Surface Weapons Center, at the White Oak Laboratory, Silver Spring, MD; the Naval Surface Warfare Center, at Indian Head, MD; the Air Force Research Laboratory, AFRL/MNME, at Eglin Air Force Base, FL; and the Center for Energetic Concepts Development (CECD), University of Maryland, at College Park.

References

- [1] R.W. Armstrong and W.L. Elban, Dislocations in Energetic Crystals, In: **Dislocations in Solids**, F.R.N. Nabarro and J.P. Hirth (Eds.), Elsevier B.V., Amsterdam, The Netherlands, 2004, Vol. 12, Chap. 69, p. 403.
- [2] H. Klapper, In: **Characterization of Crystal Growth Defects by X-ray Methods**, B.K. Tanner and H.K. Bowen (Eds.), Plenum Press, N.Y., 1980, p. 133.
- [3] E.N. Farabaugh, Ph.D. Thesis, University of Maryland, 1977; see R.W. Armstrong, In: **Crystal Properties and Preparation**, Trans Tech Publ., Switzerland, 1988, Vol.16, p. 1.
- [4] A.C. van der Steen and W. Duvalois, In: **ONR/TNO Workshop on Desensitization of Explosives and Propellants** A.C. Van de Steen (Ed.), TNO Prins Maurits Laboratory, Rijswijk, The Netherlands, 1991. Vol. 3, p. 1
- [5] R.W. Armstrong, **J. de Phys. IV-Coll. 5** (1995) C4-89.
- [6] I.T. McDermott and P.P. Phakey, **J. Appl. Phys.** 4 (1971) 479; **Phys. Stat. Sol. (a)** 8 (1971) 505.
- [7] A.R. Lang, In: **Diffraction and Imaging Techniques in Materials Science**, S. Amelinckx, R. Gevers and J. van Landuyt (Eds.), North-Holland publ., Amsterdam, 1978, Vol. II, p. 678.
- [8] J.P. Hirth and J. Lothe. **Theory of Dislocations**, McGraw-Hill Book Co., NY, 1968, Part 2, p. 201.
- [9] R.W. Armstrong and W.L. Elban, **Mater. Sci. Eng.** A111 (1989) 35.
- [10] F.C. Frank and B.R. Lawn, **Proc. Roy. Soc. Lond.** A299 (1967) 291.

- [11] R.W. Armstrong and A.C. Raghuram, In: **The Science of Hardness Testing and Its Research Applications**, J.H. Westbrook and H. Conrad (Eds.) ASM. Metals Park, OH, 1973, p. 174.
- [12] J.T. Hagan and M.M. Chaudhri, **J. Mater. Sci.** 12 (1977) 1055.
- [13] K.-C. Yoo, R.G. Rosemeier, W.L. Elban and R.W. Armstrong, **J. Mater. Sci. Lett.** 3 (1984) 560.
- [14] W.L. Elban, R.G. Rosemeier and R.W. Armstrong, In: W.L. Elban et al., Summary Report, **Microstructural Origins of Hot Spots in RDX Explosive and Several Reference Inert Materials**, Naval Surface Weapons Center, Silver Spring, MD, 1984, Report NSWC MP 84-358.
- [15] B.R. Lawn and E.R. Fuller, **J. Mater. Sci.** 10 (1975) 2016.
- [16] W.L. Elban, **J. Mater. Sci.** 14 (1979) 1008.
- [17] B.L. Hammond and R.W. Armstrong, **Philos. Mag. (Lett.)** 57 (1988) 41.
- [18] W.L. Elban, R.W. Armstrong and T.P. Russell, **Philos. Mag.** A78 (1998) 907.
- [19] R.W. Armstrong and W.H. Robinson, **New Zealand J. Sci.** 17 (1974) 429.
- [20] B.R. Lawn, **J. Appl. Phys.** 39 (1968) 4828.
- [21] R.W. Armstrong and W.L. Elban, In: **ONR Workshop on Energetic Material Initiation Fundamentals**, Los Alamos Nat. Lab., Chem. Publ. Inform. Agency, 1987, CPIA Publ. 475, p. 171.
- [22] J.J. Dick, R.N. Mulford, W.J. Spencer, D.R. Pettit, E. Garcia and D.C. Shaw, **J. Appl. Phys.** 70 (1991) 3572.
- [23] J.C. Hoffsommer, D.J. Glover and W.L. Elban, **J. Energetic Mater.** 3 (1985) 149.
- [24] R. Behrens Jr. and S. Bulushu, **J. Phys. Chem.** 96, (1992) 8877.
- [25] J.J. Gilman, In: **Synthesis, Characterization, and Properties of Energetic/Reactive Nanomaterials**, R.W. Armstrong, N.N. Thadhani, W.H. Wilson, J.J. Gilman and R.L. Simpson (Eds.) Materials Research Society, Warrendale, PA, 2004, Proc. Vol. 800, p. 287.
- [26] F.P. Bowden and A.D. Yoffe, **Initiation and Growth of Explosion in Liquids and Solids**, Cambridge University Press, London, 1952; **Fast Reactions in Solids**, Butterworths Scientific Publ., London, 1958.

- [27] S.N. Heavens and J.E. Field, **Proc. Roy. Soc. Lond.**, A338 (1974) 77.
- [28] R.W. Armstrong, C.S. Coffey and W.L. Elban, **Acta Metall.** 30 (1982) 2111.
- [29] R.W. Armstrong, In: **Encyclopedia of Engineering Materials: Science and Technology – Updates**, K.H.J. Bischow, R.W. Cahn, M.C. Flemings, E.J. Kramer, S. Mahajan and P. Veysiere (Eds), Elsevier Sci. Ltd., Oxford, UK, 2005, in print.
- [30] R.W. Armstrong, C.S. Coffey, V.F. DeVost and W.L. Elban, **J. Appl. Phys.**, 68 (1990) 979.
- [31] A.T. Nielson, Impact Sensitivity Versus Particle Size for RDX and Octanitrobenzidine (CL-12), **Working Group Meeting on Sensitivity of Explosives**, Center for Energy Technology and Research, New Mexico Institute of Technology, Socorro, 1987, p. 256.
- [32] R.W. Armstrong, K. Kline, M.P. Kramer and W.H. Wilson, In: **Twenty-Ninth International Pyrotechnics Seminar Proceedings**, F.J. Schelling (Ed.), IPSUSA, Inc., 2002, p. 239 (Abstract for unpublished presentation).
- [33] R.W. Armstrong, A.L. Ramaswamy and J.E. Field, In: **ONR/SNPE/ONERA Workshop on Combustion Mechanisms**, R.W. Armstrong (Ed.) ONR, London, UK, 1991, p. 168.
- [34] R.W. Armstrong, C.F. Clark and W.L. Elban, In: **Combustion of Energetic Materials**, K.K. Kuo and L. DeLuca (Eds.) Begell House, Inc., NY, 2003, p. 354.
- [35] K.A. Gonthier, **Modeling and analysis of reactive compaction for granular energetic solids**, Technical Report AFRL-MN-EG-TR-2001-7091, Eglin AFB, August, 2001.
- [36]. S.J. Jacobs, H.W. Sandusky and W.L. Elban, **Powder Technology**, 89 (1996) 209.
- [37] G.T. Gray III, M.A. Meyers, N.N. Thadhani, and K.S. Vecchio, **Symposium on Dynamic Deformation**, Metall. Mater. Trans. 35A (2004) pp. 2542-2745.
- [38] C.S. Smith, **Trans. TMS-AIME**, 212 (1958) 574.
- [39] W. Arnold, **Dynamische Werkstoffverhalten von Armco-Eisen bei Stosswellenbelastung**, Fortschritt-Berichte VDI-Verlag GmbH, Dusseldorf Germany, 1992.
- [40] R.W. Armstrong, W. Arnold, and F.J. Zerilli, In: **International Workshop on New Models and Hydrocodes for Shock Wave Processes in Condensed Matter**, Edinburgh, UK, 2002, Chemical Physics (Russian), in print.

- [41] **Approches Microscopique et Macroscopique des Detonations**, S. Odier (Ed.) J. de Physique, Coll C4, Suppl. 9, 48 (1987) pp. 1-433.
- [42] J.J. Gilman, **Philos. Mag. B**, 67 (1993) 207; **Philos. Mag. B**, 71 (1995) 1057.
- [43] R.W. Armstrong, H.W. Sandusky and R.S. Miller, In: **ONR Workshop on Dynamic Deformation, Fracture and Transient Combustion**, Chemical Propulsion Information Agency, 1987, CPIA Publ. 474, p. 77.
- [44] F.A. Bandak, R.W. Armstrong and A.S. Douglas, **Phys. Rev. B**, 46 (1992) 3228.
- [45] F.A. Bandak, D.H. Tsai, R.W. Armstrong and A.S. Douglas, **Phys. Rev. B**, 47 (1993) 11681.
- [46] D.H. Lassila, T. Shien, B.Y. Cao and M.A. Meyers, **Metall. Mater. Trans.** 35A, (2004) 2729.
- [47] D.H. Tsai, **J. Chem. Phys.** 95 (1991) 7497.
- [48] D.H. Tsai and R.W. Armstrong, **J. Phys. Chem.** 98 (1994) 10997.
- [49] T.C. Germann, D. Tanguy, B.L. Holian, T.S. Lomdahl, M. Mareschal and R. Ravelo, **Metall. Mater. Trans.**, 35A (2004) 2609.
- [50] J.J. Dick, **Appl. Phys. Lett.** 60 (1992) 2494.